Original Article

Journal of Intelligent Material Systems and Structures

Journal of Intelligent Material Systems and Structures
0(0) 1–12

DOI: 10.1177/1045389X13508330
jim.sagepub.com
SAGE

Bistable electromagnetic generator based on buckled beams for vibration energy harvesting

Francesco Cottone[1], Philippe Basset[1], Helios Vocca[2], Luca Gammaitoni[2] and Tarik Bourouina[1]

Abstract

Bistable piezoelectric generators have been demonstrated to outperform linear spring–mass–damper systems in terms of frequency bandwidth and harvested power from wideband vibrations. In this work, a nonlinear vibration energy harvester consisting of clamped–clamped buckled beams combined with a four-pole magnet across coil generator is investigated. By buckling the support beams, an elastic Duffing potential is provided so that the seismic mass can pass from being dynamically monostable to bistable. A theoretical model of the system is presented, and experimental tests are performed on a prototype. In the unbuckled state, the device exhibits higher maximum power at resonance than in the buckled, but, in general, no significant difference is noted in terms of average harvested power between monostable and bistable regimes under harmonic and band-limited stochastic vibrations. However, for an optimal acceleration level, the bistable configuration shows a factor of 2.5 times wider bandwidth and higher power outside from the natural resonance as compared with the monostable regime. It is also observed that the benefits of bistable dynamics mostly depend on the ratio between the characteristic cutoff frequency of the electrical circuit and the mechanical resonance.

Keywords

Vibration energy harvesting, bistable systems, buckled beams, electromagnetic generators

Introduction

The reduction in power needs of wireless sensor nodes as well as small smart electronic devices has, in recent years, met the capability of small generators to harvest from various ambient energy sources like solar, temperature gradient, wind, radio frequencies (RF), and vibrations. This is mainly due to the rapid improvement of power-aware and energy-efficient electronics at various technological levels: material, design, components, and circuitry (Amirtharajah et al., 2000; Bilbao et al., 2011). Latest wireless sensor nodes are able to operate when powered only with few tens of microwatts.

The main problem of vibration harvesting is the variability of the power spectral density (PSD), both in terms of time and frequency content. Most generators are indeed optimized to work only at specific frequencies, thus the applications are limited. Commercial vibration energy harvesters (VEHs) are generally application designed in order to maximize the performance. However, for a wideband operation, additional features need to be added to the typical linear spring–mass system used in resonant VEH. Vibration harvesters based on linear oscillators must resonate at their natural frequency in order to maximize the power. This represents the main limit of linear systems. In fact, to be efficient over a wide frequency range, they must be capable of self-tuning and adaptation to variable acceleration levels (Ayala-Garcia et al., 2013; Eichhorn et al., 2011; Galayko et al., 2008). But these techniques require a complex active circuit which consumes additional power. Another method for widening the frequency response is the use of an oscillator array with different resonances; therefore, the overall response covers a larger frequency interval (Koyama and Nakamura, 2010; Shan et al., 2010; Xue et al., 2008). However, in that case, the overall power density per unit of device volume decreases. Multimodal energy harvesting with a single oscillator has also been investigated (Yang et al., 2009).

[1]Université Paris-Est, ESYCOM, ESIEE Paris, France
[2]Department of Physics, University of Perugia, Perugia, Italy

Corresponding author:
Francesco Cottone, Université Paris-Est, ESYCOM, ESIEE Paris, Noisy-le-Grand, F-93162, France.
Email: f.cottone@esiee.fr

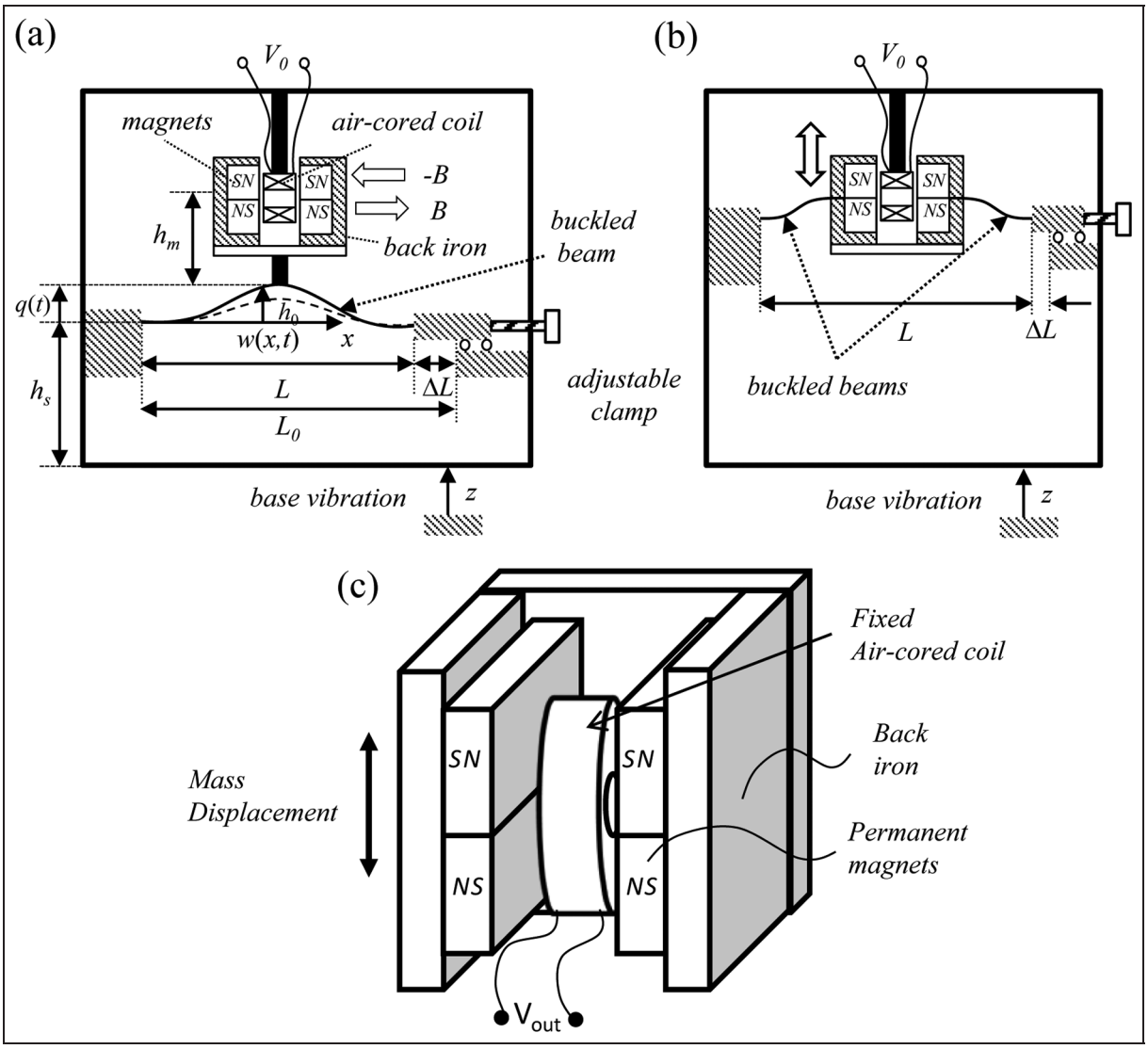

Figure 1. Model of the buckled-beam BEMG with two clamping configurations: (a) centrally loaded buckled-beam clamping, (b) double buckled-beam clamping, and (c) schematics of the magnets–coil arrangement.
BEMG: beam electromagnetic generator.

The exploitation of nonlinear systems can also be used for improving the spectral bandwidth (BW) of VEHs. It was proposed for electromagnetic transduction (Burrow and Clare, 2007) and by the authors of this work (Cottone et al., 2009) via piezoelectric generators. Such an approach of using an external force to create a quartic potential was also investigated by other researchers (Erturk and Inman, 2010; Stanton et al., 2010). Under wide spectrum noise, the superiority of bistable systems with respect to linear resonators in terms of maximum power and frequency response was proven to be up to an order of magnitude higher. Other nonlinear techniques that make use of mechanical stoppers have been shown to be advantageous to enlarge the BW generators (Guillemet et al., 2013; Soliman et al., 2008). A good classification of different nonlinear techniques is described in Tang et al. (2010).

In this article, we analyze an inertial electromagnetic generator (EMG) wherein buckled steel beams are employed to work as an equivalent nonlinear bistable spring in order to make the seismic mass vibrating within an elastic quartic potential. The authors have already demonstrated this concept for a piezoelectric generator (Cottone et al., 2012). The aim of this work is to understand the effect of bistability for an electromagnetic VEH. In particular, we investigate the system in two different arrangements: on one hand, with a single clamped–clamped steel beam wherein the seismic mass is centrally fixed (Figure 1(a)) and, on the other hand, with two separate beams which are laterally clamped to the seismic mass and aligned to its center (Figure 1(b)). Although these two configurations are similar, the mechanical resonance of the system changes as the clamp-to-clamp distance is kept constant. Thus, we

study how the bistability influences the system response when its mechanical resonance is far and close to the circuit cutoff frequency. The first arrangement lowers the frequency response and eases the snapping between the two states, although the mass is unstable. The second suspension configuration is stable but with higher frequency response, considering the same clamp-to-clamp length. The comparison will be made between the unbuckled and buckled states for each configuration, under harmonic vibration and band-limited noise.

The theoretical model of the buckled-beam electromagnetic generator (BEMG) will be explained in section "Theoretical framework." Then, the description of the prototype and experimental characterization will be discussed in section "Description of the prototype." Section "Experimental results" will show the performance comparison of resonant unbuckled- versus buckled-beam configuration under frequency sweep-in-sine excitation and band-limited colored noise. Section "Conclusion" will finally include the conclusions of this work.

Theoretical framework

Description of the model

Figure 1 illustrates the model of the buckled-BEMG sketched with two clamping configurations: (a) where the seismic mass, which is composed by the magnet housing, is fixed to the center of a single buckled beam and (b) where it is doubly clamped with two buckled beams at its sides. In both configurations, the position of one clamp (right) of the support can be adjusted by means of a micrometric screw. By decreasing the initial clamp-to-clamp distance L0 by a certain quantity deltaL, the axial compression increases such that, over a critical value, the support beam becomes buckled. The distance between the beam ends is named $L = L_0$-deltaL. The unbuckled state of the beam corresponds to the uncompressed condition $L = L_0$. Thus, the support beams can be placed in a buckled state, whereas the unbuckled state corresponds to the uncompressed condition $L = L_0$.

The movable part of the generator is composed of four permanent magnets having their poles aligned horizontally, such that the top couple of magnets produce a magnetic field B in the opposite direction with respect to that of the bottom magnets (Figure 1(c)). This arrangement, as formerly proposed by El-Hami et al. (2001), permits to increase the magnetic flux linkage gradient $d\Phi(B)/dz$ along the vertical axis z. The magnet support is made of soft iron in order to confine the magnetic flux, and at the same time, it increases the total seismic mass of the harvester. The stator is made of an air-cored coil of horizontal loop axis located within the magnets gap and is attached to the rigid housing of the device. Thus, the movement of the magnetic element relative to the coil generates the electromotive force V_0.

Governing equations

Hereafter, the theoretical framework will be only developed for the configuration of single centrally loaded buckled beam (Figure 1(a)). The partial differential equation that governs the vertical deflection $w(x, t)$ of a post-buckled beam undergoing compressive axial force P was extensively investigated in Emam and Nayfeh (2004) and Reddy (2004). It is given by

$$m(x)\frac{\partial^2 w}{\partial t^2} + c\frac{\partial w}{\partial t} + EI\frac{\partial^4 w}{\partial x^4} + \left(P - \frac{EA}{2L}\int_0^L \left(\frac{\partial w}{\partial x}\right)^2 dx\right)\frac{\partial^2 w}{\partial x^2} = -m(x)\left(\frac{d^2 z}{dt^2} + g\right) \quad (1)$$

where

$$m(x) = \rho A + M\delta(x - L/2) \quad (2)$$

is the total mass per unit length and M is the seismic mass given by the magnets housing; δ is the Dirac delta function; t is time; x is the horizontal axis coordinate; z is the vertical position of the base; E and I are the beam Young's modulus and second moment of inertia, respectively; ρ, A, and g are the mass density, cross-sectional area of the beam, and gravitational acceleration ($g = 9.81$ m s^{-2}), respectively; and c accounts for the mechanical viscous damping.

As this work only aims at investigating the concept of bistability when applied to EMGs, a deeper theoretical analysis of buckled beams accounting for asymmetries will not be treated here. Therefore, we just consider the first vibration mode as dominant in the Galerkin expansion of the total deflection function

$$w(x,t) = w_1(x) + v(x,t),\ v(x,t) = \sum_{i=1}^{N} r_i(t)\varphi_i(x) \quad (3)$$

where N is the number of retained modes of interest, $v(x,t)$ is the time-dependent deflection around the initial shape $w_1(x) = h_0\psi(x)$ with initial midpoint buckling height h_0, $\phi_i(x)$ are the position-dependent mode shapes of the beam, and $r_i(t)$ are generalized displacement of the time-dependent mode shapes. By retaining only the first mode the expression (3) results

$$w(x,t) = h_0\psi(x) + \psi(x)r(t) \quad (4)$$

where $\psi(x) = (1 - \cos(2\pi x/L))/2$ is the initial shape function (Emam and Nayfeh, 2004).

In place of $r(t)$, we now define the generalized coordinate $q(t) = h_0 + r(t)$, which is the time-dependent midpoint height of the beam. Hence, $w(x,t) = q(t)\psi(x)$ and by replacing it into equation (1) and evaluating at $x = L/2$, a single degree-of-freedom (1-DOF) differential equation is obtained

$$M_{eq}\ddot{q}(t) + \vartheta\dot{q}(t) + k_1 q(t) + k_3 q(t)^3 = -M_{eq}(\ddot{z}(t) + g) \tag{5}$$

where overdots are time derivatives. M_{eq} and ϑ are the effective seismic mass of the oscillator and effective viscous damping, respectively. k_1 and k_3 represent linear and nonlinear terms of the equivalent spring stiffness, respectively. These parameters are derived by the following expressions

$$\begin{aligned} M_{eq} &= \rho A \int_0^L \psi(x)^2 dx + M\psi(L/2)^2 && \text{(a)} \\ \vartheta &= c \int_0^L \psi(x)^2 dx && \text{(b)} \\ k_1 &= EI \int_0^L [\psi(x)'']^2 dx - P \int_0^L [\psi(x)']^2 dx && \text{(c)} \\ k_3 &= \frac{EA}{2L} \int_0^L [\psi(x)']^2 dx && \text{(d)} \end{aligned} \tag{6}$$

Primes represent the derivative with respect to x. The total compressive force P is calculated by the following relations

$$\begin{aligned} P &= P_{cr} + \frac{EA}{2L} \int_0^L \left(\frac{\partial h_0 \psi(x)}{\partial x} \right)^2 dx && \text{(a)} \\ P_{cr} &= \frac{4\pi^2 EI}{L^2} && \text{(b)} \end{aligned} \tag{7}$$

where P_{cr} is the critical buckling load.

Let us now include the magnetic force arising from the movement of the magnets relative to the inner coil. When the coil is shunted to an electrical load R_L, the magnetic force along z is given by $F_m = -Bli$, where B is the modulus of the magnetic field component along x within the gap of each couple of magnets, l is the total length of the active coil wire within the magnetic field, and i is the current flowing through the load. The induced electromotive force is equal to $V_0 = Bl(dq/dt)$ from Faraday's law, where dq/dt is the vertical velocity of the seismic mass. By naming R_c and L_c the internal resistance and the self-inductance of the coil, respectively, the voltage across the resistive load is given by

$$V = V_0 - R_c i - L_c(di/dt) \tag{8}$$

By Ohm's law, the current can be rewritten in terms of load voltage $i = V/R_L$ so that the coupled closed-form equations governing both dynamical and electrical behavior of the BEMG are obtained as

$$\begin{aligned} &M_{eq}\ddot{q}(t) + \vartheta\dot{q}(t) + k_1 q(t) + k_3 q(t)^3 + \alpha V(t) \\ &= -M_{eq}(\ddot{z}(t) + g) \end{aligned} \tag{9}$$

$$\dot{V}(t) + (\omega_L + \omega_R)V(t) = \omega_R \lambda \dot{q}(t) \tag{10}$$

in which α is the electromechanical coupling factor; ω_L and ω_R are the characteristic cutoff frequencies of the electrical circuit of the system relative to the coil resistance R_c and to external resistive load R_L, respectively; and λ is the electromagnetic conversion factor. They are defined by the physical system parameters as follows

$$\begin{aligned} \alpha &= \frac{Bl}{R_L} \quad \text{(a)} \quad \lambda = Bl \quad \text{(b)} \\ \omega_R &= \frac{R_L}{L_c} \quad \text{(c)} \quad \omega_L = \frac{R_c}{L_c} \quad \text{(d)} \end{aligned} \tag{11}$$

The corresponding nondimensional equations (6) and (7) are then derived as detailed in Appendix 1

$$\frac{d^2\tilde{q}(\tau)}{d\tau^2} + \frac{1}{Q}\frac{d\tilde{q}(\tau)}{d\tau} + \tilde{q}(\tau) + \tilde{q}^3(\tau) + \tilde{V}(\tau) = -\frac{d^2\tilde{y}(\tau)}{d\tau^2} \tag{12}$$

$$\frac{d\tilde{V}(\tau)}{d\tau} + \frac{1}{\gamma}\tilde{V}(\tau) = k_{em}^2 \frac{d\tilde{q}}{d\tau} \tag{13}$$

in which there are only three independent dimensionless parameters: the mechanical quality factor Q, the characteristic ratio between the mechanical resonance and electrical cutoff frequency ratio which is equal to

$$\gamma = \frac{\omega_0}{\omega_R + \omega_L} \tag{14}$$

and the nondimensional electromechanical coupling factor of the system

$$k_{em}^2 = \frac{\lambda^2}{k_1 L_c} = \frac{(Bl)^2}{k_1 L_c} \tag{15}$$

Description of the prototype

In this section, the above coupled nondimensional equations are solved in the time domain. Numerical integration is carried out by using modified Euler–Marujama method implemented in MATLAB®. The input excitations are harmonic vibrations and exponentially correlated band-limited noise. The numerical solutions are based on the identified physical parameters deduced from the prototype. The average electrical power is calculated within the interval $[t_0, t_1]$ by using the formula

$$P_{avg} = \frac{1}{t_1 - t_0} \int_{t_0}^{t_1} \frac{V^2(t)}{R_L} dt \tag{16}$$

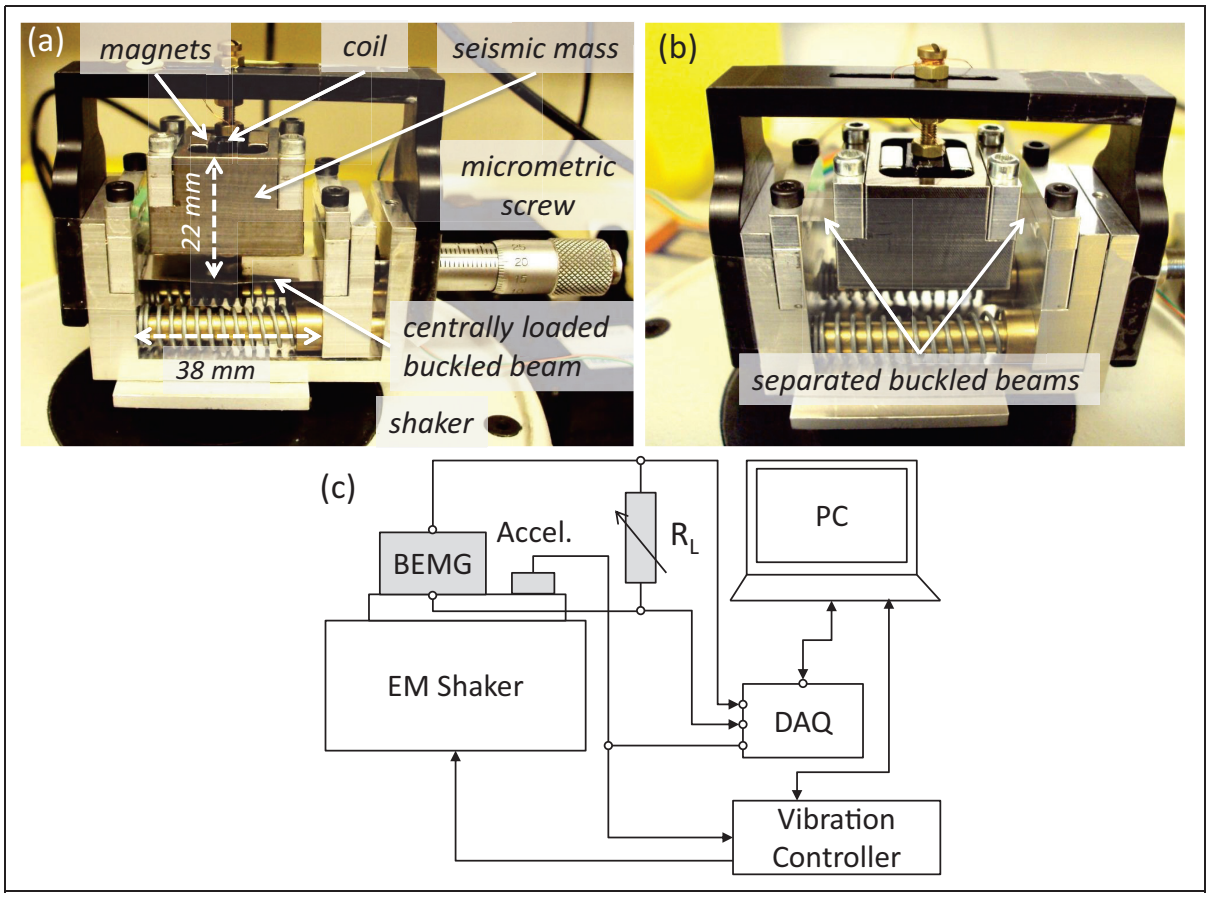

Figure 2. Photographs of the BEMG prototype for the (a) single centrally loaded-beam clamping configuration, (b) double-beam clamping configuration, and (c) scheme of the testing equipment.
BEMG: beam electromagnetic generator; PC: personal computer; DAQ: data acquisition.

BEMG and experimental setup

The fabricated prototype is illustrated in Figure 2(a) and (b) for the centrally loaded beam and separated beams arrangement, respectively. The active parts (springs + magnet housing + coil) measure an overall size of 38 mm × 22 mm × 25 mm. Four neodymium-iron-boron (NdFeB) magnets are hosted in the iron support, which constitutes the moving mass. The coil is fixed to the embodiment by means of a nylon support which operates as a low friction rail. Its vertical position can be regulated by a screw. The coil operates as stator being rigidly placed in between the magnets with its axes parallel to the magnetic field along the horizontal direction.

By adjusting the movable right clamp, it is possible to change the compressive axial load on the steel beam, so that the oscillator passes from monostable to bistable dynamical regime. When shaken, the magnetic element slides vertically around the nylon support of the coil providing a better stability to the seismic mass.

Figure 2(c) shows the schematic diagram of the used experimental equipment. Vibrations are provided to the energy harvesting device by means of an electromagnetic shaker. The base acceleration is monitored by using an accelerometer with 800 mV/g of sensitivity. The electrical terminals of the coil are connected in series to a resistance. All the signals are acquired by a data acquisition card connected to a personal computer (PC) run by a LabVIEW program. The vibration signal is handled by a vibration controller through the feedback of the accelerometer for the sweep-in-sine tests.

System characterization

The physical parameters of the fabricated harvester are listed in Table 1 and the calculated parameters of the theoretical model are shown in Table 2. The effective quality factor, Q, was characterized through the method of the logarithmic decrement by using a step-like vibration (Palm, 2007). The electromagnetic coupling factor α was obtained by using equation (11a). Note that this is only an approximation because the electromagnetic force is nonlinear and depends on the position of the oscillating magnet. In addition, it is not possible to determine the effective coupling factor at open circuit due to eddy currents.

Table 1. Measured physical parameters of the prototype.

Parameter, symbol	Value	Parameter, symbol	Value
Magnetic element		*Beam spring element*	
Material	NdFeB (N42)	Material	Steel C-70
Magnetic field, B	0.42 T	Unbuckled length, L_0	37.9×10^{-3} m
Magnet size	$10 \times 10 \times 3$ mm^3	Width, b	12.7×10^{-3} m
Coil wire diameter, w_d	0.08×10^{-3} m	Thickness, t_b	0.09×10^{-3} m
Coil wire length, w_l	31.4 m	Density, ρ_b	7850 kg/m^3
Coil self-inductance, L_c	7.66 mH	Young's modulus, E_b	2×10^{11} Pa
Coil resistance, R_c	106 Ω		

Table 2. Parameters of the theoretical model of Figure 2(a).

Parameter, symbol	Value
Resonant frequencies, f_u; f_b	51.7 Hz*; 47 Hz*; 52 Hz**; 48 Hz**
Quality factor (open circuit), Q	29*
Equivalent mass, M_{eq}	72.3×10^{-3} kg**
Linear stiffness, k_1 (unbuckled); k_1 (buckled)	601*; -2×10^3 N/m*
Nonlinear stiffness, k_3	5.82×10^{10} N/m^3*
Coupling factor, α (at R_L = 112 Ω)	1.17×10^{-1} N/V*
Cutoff frequency, f_c	2.3 kHz*

*Calculated; **measured.

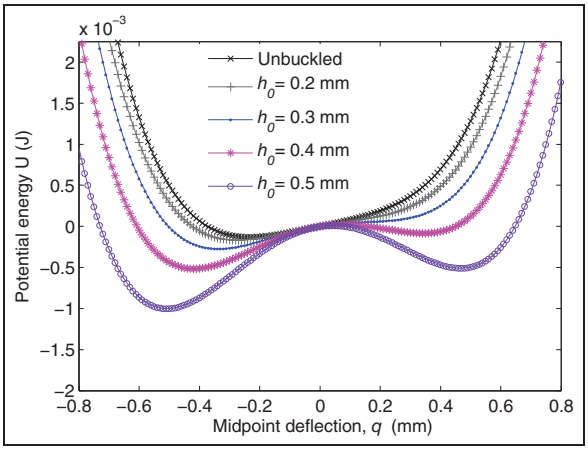

Figure 3. Potential energy of the system for increasing values of buckling height h_0.

The total potential energy of the system is expressed by

$$U(q) = \frac{1}{4}k_3q^4 + \frac{1}{2}k_1q^2 + M_{eq}gq \qquad (17)$$

In the unbuckled case, the stiffness coefficient k_1 is positive and the system oscillates around its unique stability point which corresponds to a midspan deflection $q = 0$. When a compression is applied over the critical axial load, the beam is set in the buckled state. In this condition, the stiffness coefficient k_1 is negative. The initial axial load P can be determined by measuring the buckling height h_0 and using equation (7).

Figure 3 shows the graph of the potential energy for various buckling height. The double well potential is tilted due to the gravitational force, and the solutions for the two stability positions have a complicated expression. However, if we assume the gravity force is negligible, the two stability positions of the system are $q_\pm = \pm(|k_1|/k_3)^{1/2}$.

Experimental results

In section "Harmonic excitation," the test results under harmonic excitation are presented for the generator configured with the single support beam arrangement shown in Figure 2(a). In this case, relatively low accelerations are required for the mass to overcome the barrier height of the Duffing potential compared to the separated buckled beam arrangement (Figure 2(b)). A first test was performed by monitoring the output voltage for different resistance loadings at resonance. Subsequently, two test sessions with frequency sweep-up and sweep-down sinusoidal excitation were performed at open circuit and with optimal load. Each measurement was retrieved both for the unbuckled and buckled beam cases.

In section "Band-limited noise," the tests are then performed under band-limited noise for both clamping arrangements. Hereafter, simulations and experimental values will be compared within the same scales but in different graphs to avoid confusion in overlapping many curves.

Harmonic excitation

Figure 4(a) illustrates the generated root mean square (*rms*) voltage across different load resistances ranging from 23 Ω to 4.6 kΩ. The system was shaken at the measured peak resonances equal to $f_u = 52$ Hz and $f_b = 48$ Hz for unbuckled and buckled configurations (with $h_0 = 0.4$ mm), respectively, at $\sigma = 0.32\ g_{rms}$ of

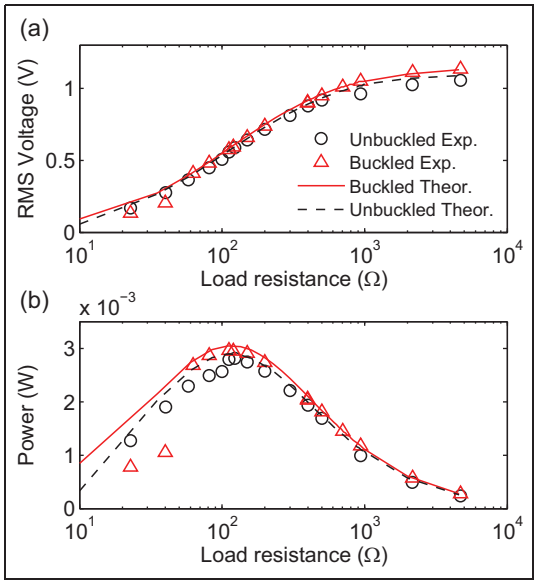

Figure 4. (a) The *rms* voltage for harmonic excitation at first resonance f_u = 52 Hz and f_b = 48 Hz, respectively, for unbuckled and buckled configurations (with h_0 = 0.4 mm) versus load resistance at 0.32 g_{rms} of base acceleration. (b) Electrical average power versus load resistance. Theoretical curve is calculated for the unbuckled case.

base acceleration (Table 2). The effective value of the magnetic field seen by the coil was deduced by fitting the experimental data with theoretical model, and it is found to be $B = 0.42$ T. In both unbuckled and buckled states, the optimal load resistance results to be 112 Ω, at which the maximum average electrical power is $P_{max} = 2.96$ mW.

The theoretical curve is calculated for the unbuckled state, but it is also in good agreement with the buckled one. A small discrepancy appears for very small loads (22.8 and 40 Ω). No sensible improvement in terms of maximum power or load BW is achieved in the buckled state when exciting at main natural frequency. This behavior differs from the case of piezoelectric transduction as seen in Cottone et al. (2012). The reason of the lack in power gain comes from the small time constant of the equivalent circuit, namely, $\tau = L_c/(R_L + R_c) = 34$ μs. Accordingly, the characteristic cutoff frequency of the equivalent high-pass filter of the circuit results to be $f_c = 1/(2\pi\tau) = 2.3$ kHz. This is much greater than the mechanical resonances $f_u = 52$ Hz and $f_b = 48$ Hz. Hence, the characteristic frequency ratio $\gamma \ll 1$, while it can be $\gamma > 1$ for piezoelectric systems. As a consequence, the second term at the left side of equation (24) is not negligible anymore. Thus, even if the bistable dynamic yields large mass displacement, the output voltage does not increase significantly because it depends on the velocity.

Figure 5(a) and (b), respectively, presents the experimental results and numerical model of the *rms* voltage of the system at open circuit for upward and downward frequency sweeping for both unbuckled and buckled states at $\sigma = 0.32\ g_{rms}$ of acceleration. As expected, the buckling softens the effective stiffness of the oscillator. The measured peak resonance shifts from 52 to 48 Hz, while numerical simulations predict 51.7 and 47 Hz for monostable and bistable states, respectively. Both the experimental and numerical model data show multiple coexisting values in the frequency range of 35–47 Hz for the buckling state. This region corresponds to the inter-well motion of the seismic mass which snaps through the two potential minima. The frequency response of the buckled state is slightly broadened with respect to the unbuckled on downward sweeping, while for upward sweeping, the band is squeezed. This hysteresis occurs because the excitation level is not enough for allowing the mass to overcome the potential barrier. In fact, in the upward sweeping, the gravitational force confines the mass to stay in the lower well of the quartic potential. This phenomenon disappeared when increasing acceleration or decreasing the buckling height h_0, as shown in Figure 6.

Figure 5(c) and (d) shows the frequency sweep of the *rms* output voltage when applying the optimal resistive load $R_{opt} = 112$ Ω found at resonance, respectively, for experimental and simulated models. Even in this case, the numerical model results to be in good agreement with experimental data. As for the open circuit case, the hysteresis due to the bistability combined with the gravitational force is reproduced. However, the simulations present some discrepancies with respect to experimental data below 30 Hz. Simulated models exhibit subresonances around 22 and 28 Hz. Experimental data also outline only a small plateau in correspondence of predicted subresonances around similar frequencies: 25 and 33 Hz for unbuckled and buckled states, respectively. The effects are related to the approximation of a constant magnetic field seen by the top and bottom half of the coil. In addition, nonlinear loss effects have not been accounted as in Sebald et al. (2011).

The frequency response of the unbuckled state appears not much different from the buckled one because the buckling height was chosen relatively small in order to let the system crossing the potential barrier for low accelerations. The BW of the bistable system exhibits very sharp boundaries which restrict the efficiency region in between 33 and 48 Hz. Although the unbuckled state exhibits a higher maximum value at resonance, the buckled one performs better in the frequency range between 34 and 49 Hz. Both experiments and simulations present an output enhancement at frequencies beyond 57 Hz. The experimental power enhancement of the buckled system varies along this frequency range and reaches a maximum of 115% at 85 Hz. This phenomenon is attributed to the vibrations of the seismic mass when it is confined in one of the two stability positions. The intra-well resonance of the

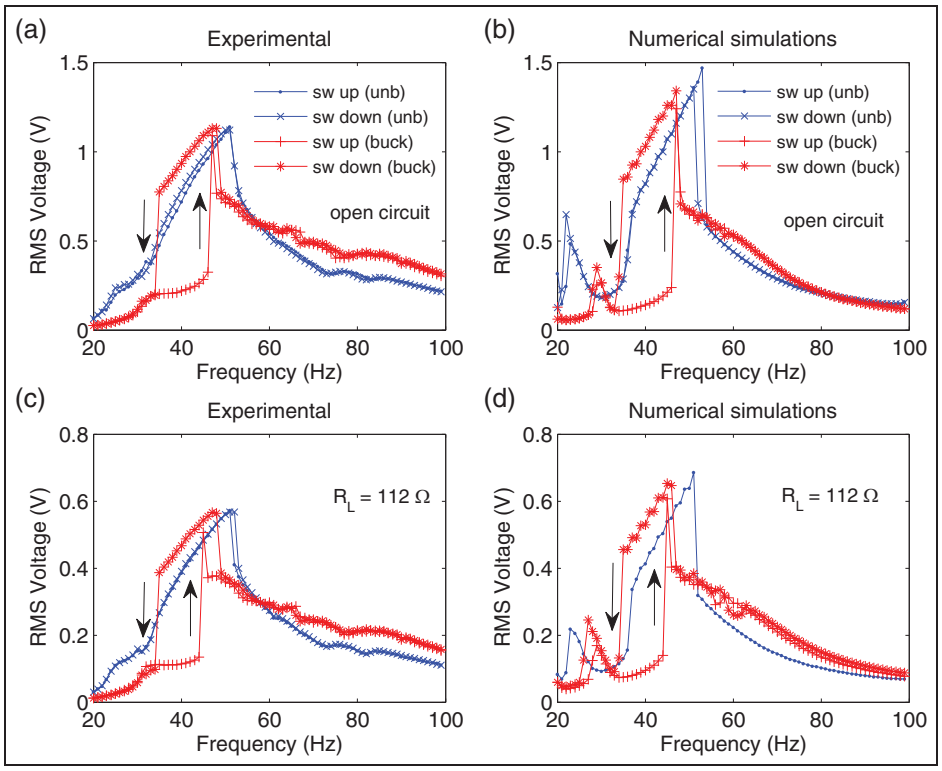

Figure 5. Experimental (left column) and simulated (right column) results of frequency sweep up and sweep down in both unbuckled and buckled (h_0 = 0.5 mm) configurations. (a and b) open-circuit *rms* voltage and (c and d) *rms* voltage across the optimal load resistance R_L = 112 Ω. In all cases, the acceleration amplitude is σ = 0.32 g_{rms}.
rms: root mean square.

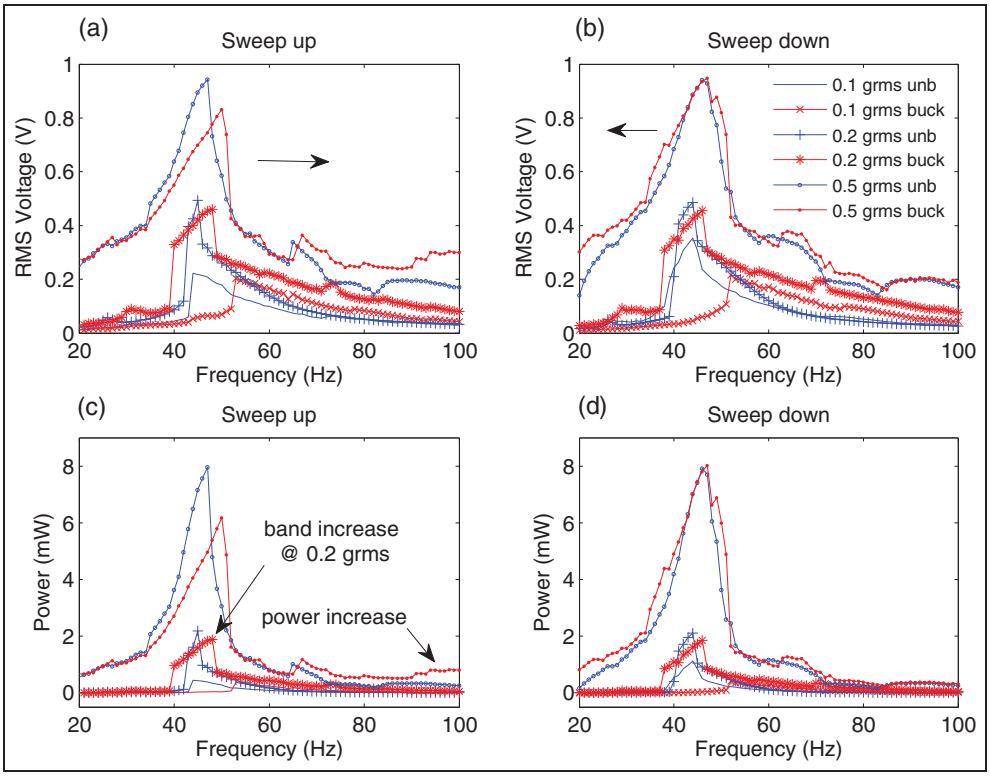

Figure 6. Experimental comparison of unbuckled- and buckled-beam (h_0 = 0.3 mm) generators for up (left column) and down (right column) frequency sweeps with acceleration amplitudes of 0.1, 0.2, and 0.5 g_{rms}. (a and b) *rms* voltage and (c and d) the corresponding power dissipated across the optimal load resistance R_L = 112 Ω.
rms: root mean square.

buckled state is higher than the natural frequency of the unbuckled state. Therefore, the frequency response is shifted to right, resulting in a greater response in the high frequency range.

Another comparison between unbuckled and buckled states, but for various acceleration levels, is shown in Figure 6. The initial buckling height is 0.3 mm. Frequency up and down sweeps correspond to the first and second columns, respectively. In each column, the output *rms* voltage (Figure 6(a) and (b)) and the corresponding power (Figure 6(c) and (d)) dissipated to the optimal load of 112 Ω are presented at 0.1, 0.2, and 0.5 g_{rms} of base acceleration. It is important to observe that even if the maximum power results higher at resonance for the unbuckled state, the buckled one provides a larger BW at the intermediate acceleration of 0.2 g_{rms}. Moreover, up to a power gain of a factor 3 occurs in the bistable state off the main resonance, in the interval of 67−100 Hz. Few sub- and super-harmonics appear around 33 and 66 Hz, respectively. This phenomenon is typical of nonlinear vibrating systems as discussed in Nayfeh et al. (1999).

A maximum power of 8 mW resulted at 0.5 g_{rms}, which is quite a remarkable value for powering commercial wireless electronics. We can also evaluate the power frequency BW and the bandwidth figure of merit (BWFoM) in order to compare the performance in both configurations by using the definition in Sebald et al. (2011)

$$\mathrm{BW} = \frac{f_2 - f_1}{f_0} \tag{18}$$

$$\mathrm{BWFoM} = \mathrm{BW} \times \frac{P_{max}}{\sigma^2} \tag{19}$$

where f_2, f_1 represent the half-power ($-3db$) cutoff frequencies, f_0 is the maximum power frequency, and σ is the acceleration amplitude. At 0.2 g_{rms}, the buckled system shows a frequency BW of $\mathrm{BW_b} = 20.8\%$ against the unbuckled one $\mathrm{BW_u} = 8.8\%$ resulting in a gain factor of 2.5. Besides, we can note that both configurations of the device feature very large BW responses compared to traditional cantilever-based harvesters. Indeed, typical values of BW of linear resonant VEHs range from 2% to 15% (Mitcheson et al., 2008). Furthermore, still at 0.2 g_{rms} of acceleration the BWFoM results to be 5.65 and 2.07 mW/g^2 for buckled and unbuckled generators, respectively.

Band-limited noise

In this section, the system is also investigated under exponentially correlated colored noise with the autocorrelation time $\tau_a = 0.001$ s. The input vibration consists of a stochastic noise $z(t) = \xi(t)$ with limited BW at the cutoff frequency $f_a = 1/(2\pi\tau_a) = 159$ Hz. The PSD of the input acceleration $\xi(t)$ at $\sigma = 1$ g_{rms} is shown in Figure 7. The experimental test in the following refers to an acceleration of 0.4 g_{rms}.

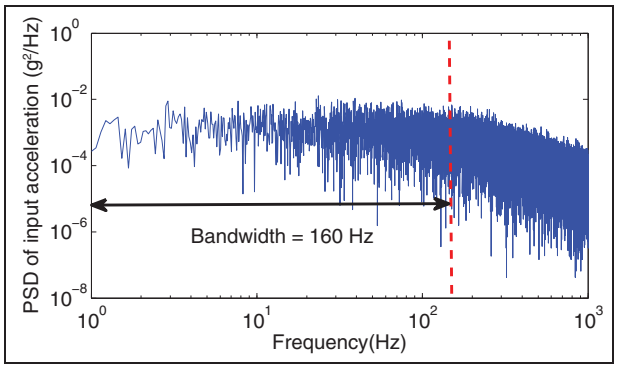

Figure 7. PSD of colored noise acceleration at 1 g_{rms} generated in 10 s at 10 kHz with bandwidth limited at f_a = 159 Hz.
PSD: power spectral density.

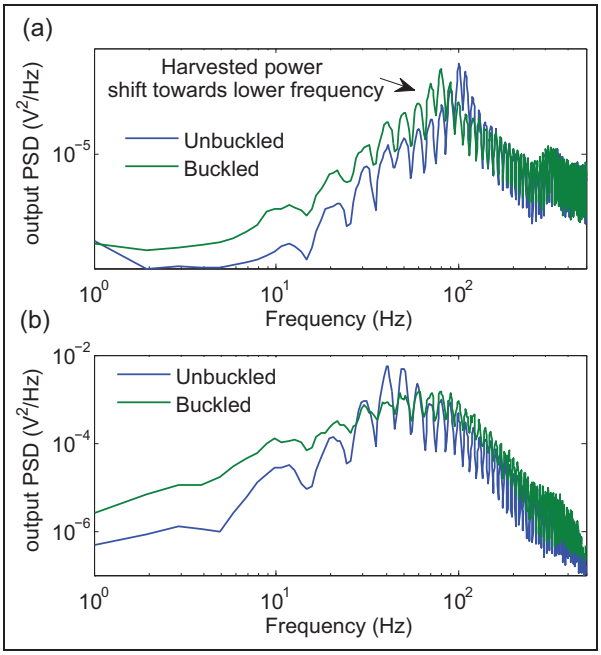

Figure 8. PSD of output voltage of the BEMG for (a) double-beam and (b) single-beam clamping arrangements at 0.4 g_{rms} of acceleration for 10 s at 10 kHz of sampling under band-limited exponentially correlated noise.
PSD: power spectral density; BEMG: beam electromagnetic generator.

Figure 8 shows the PSD of the system response that is estimated from measurements by using Welch's averaged periodogram for the two different arrangements: double- and single-beam clamping. In the buckling state of the support beams, the power response shifts by about 30 Hz toward lower frequencies showing an increase in this range.

We can also observe that the maximum power peak of the single-beam clamped system, which resonates at $f_0 \sim 50$ Hz, is mitigated under buckling state. However,

such an attenuation does not occur for the double-beam clamping arrangement. This is explained by the high-pass filtering effect of the electrical circuit. The second arrangement with double-beam suspension presents similar power peaks at higher mechanical resonances: 3.7×10^{-3} V^2/Hz at 100.6 Hz (unbuckled) and 2.7×10^{-3} V^2/Hz at 80 Hz (buckled). In the single-beam clamping configuration, the maximum electrical power dissipated through the resistance does not present any improvement under buckled state with respect to the unbuckled: 4.8×10^{-3} V^2/Hz at 50 Hz (unbuckled) and 1.2×10^{-3} V^2/Hz at 48 Hz (buckled). Nevertheless, the down shift in frequency response allows to harvest more energy at low frequency: below 27 Hz, the buckled system harvest one order of magnitude more power than the unbuckled one.

The effect of bistability on the electromagnetic harvester

Under random vibrations, the EMG appears not to benefit from bistable dynamic as much as for piezoelectric systems (Cottone et al., 2009, 2012). However, the harvesting efficiency increases at low frequency, which can be advantageous with some vibration sources (e.g. human movement). The reason of such effect is related to the ratio between the electrical cutoff frequency of the electrical circuit and the mechanical resonance, γ, which in this case results much less than 1. As a consequence, the output voltage is mainly proportional to the velocity and does not depend on the displacement amplitude. In principle, it could be possible to design the electromagnetic harvesting system in order to have parameter $\gamma > 1$. For instance, by increasing the mechanical frequency $f_0 = \omega_0/2\pi$ or decreasing the overall electrical cutoff frequency $f_c = (\omega_R + \omega_L)/2\pi$. This can be done by choosing very stiff support springs or by increasing the self-inductance of the electromagnetic inductor.

Conclusion

This work presented the design, analysis, and experimental testing of a nonlinear buckled BEMG for vibration energy harvesting. In particular, the use of a clamped–clamped beam with adjustable position of one of the two clamps allowed investigating the system in monostable and bistable dynamics, corresponding to the unbuckled and buckled beam states. In the first case, the device behaves like a resonant generator while, in the second one, it works as a bistable Duffing oscillator. The governing equations for the BEMG were derived by using first mode Galerkin expansion with the Euler beam theory. The fabricated device was tested under harmonic excitation with frequency sweeping (from 20 to 106 Hz) and under band-limited exponentially correlated noise.

In general, not much performance difference is found in terms of average harvested power between the bistable and monostable regimes, both under harmonic and band-limited stochastic vibrations. This can be attributed to the high-pass filtering effect of the equivalent electrical circuit that presents a cutoff frequency much greater than mechanical resonance.

Nevertheless, the buckled configuration of the fabricated device presents a BW enhancement of 2.5× with respect to unbuckled at intermediate acceleration of 0.2 g_{rms}. In addition, the buckled beam system performs slightly better off the resonant region with respect to the unbuckled. In fact, a power enhancement up to a factor 3× is observed above 67 Hz at 0.5 g_{rms} of base excitation. However, under monostable regime, the maximum harvested power at resonance is achieved by the monostable state.

In both buckled and unbuckled states, the device demonstrated a maximum harvested power of 8 mW at 0.5 g_{rms} of base acceleration. This value demonstrates a good potential for practical vibration-powered wireless sensing applications. Moreover, it has been proven that clamped–clamped beam design provides larger frequency response than typical cantilever-based harvesters because of the nonlinearity of the suspension. Numerical model and experimental results show a good quantitative and qualitative agreement.

Declaration of conflicting interests

The authors declare that there is no conflict of interest.

Funding

This study was supported by FP7 Marie Curie Intra-European Fellowship (IEF) funding scheme, Grant No. 275437, at ESIEE Paris, Universite' Paris-Est."

References

Amirtharajah R, Meninger S, Mur-Miranda JO, et al. (2000) A micropower programmable DSP powered using a MEMS-based vibration-to-electric energy converter. In: *2000 IEEE international solid-state circuits conference, 2000. Digest of Technical Papers. ISSCC*, San Francisco, CA, 9 February. New York: IEEE, pp. 362–363.

Ayala-Garcia I, Mitcheson P, Yeatman E, et al. (2013) Magnetic tuning of a kinetic energy harvester using variable reluctance. *Sensors and Actuators A: Physical* 189: 266–275.

Bilbao A, Hoover D, Rice J, et al. (2011) Ultra-low power wireless sensing for long-term structural health monitoring. In: *Sensors and smart structures technologies for civil, mechanical, and aerospace systems 2011*, San Diego, CA, 6 March, Article ID 798109. Bellingham, WA: SPIE.

Burrow S and Clare L (2007) A resonant generator with nonlinear compliance for energy harvesting in high vibrational

environments. In: *IEEE International electric machines & drives conference, 2007. IEMDC '07*, Antalya, Turkey, 3–5 May, pp. 715–720. New York: IEEE.

Cottone F, Gammaitoni L, Vocca H, et al. (2012) Piezoelectric buckled beams for random vibration energy harvesting. *Smart Materials & Structures* 21, DOI: 10.1088/0964-1726/21/3/035021.

Cottone F, Vocca H and Gammaitoni L (2009) Nonlinear energy harvesting. *Physical Review Letters* 102. p. 080601, reference DOI 10.1103/PhysRevLett.102.080601.

Eichhorn C, Tchagsim R, Wilhelm N, et al. (2011) A smart and self-sufficient frequency tunable vibration energy harvester. *Journal of Micromechanics and Microengineering* 21: 104003.

El-Hami M, Glynne-Jones P, White N, et al. (2001) Design and fabrication of a new vibration-based electromechanical power generator. *Sensors and Actuators A: Physical* 92: 335–342.

Emam SA and Nayfeh AH (2004) On the nonlinear dynamics of a buckled beam subjected to a primary-resonance excitation. *Nonlinear Dynamics* 35: 1–17.

Erturk A and Inman D (2010) Broadband piezoelectric power generation on high-energy orbits of the bistable Duffing oscillator with electromechanical coupling. *Journal of Sound and Vibration* 330: 2339–2353.

Galayko D, Basset P and Paracha AM (2008) Optimization and AMS modeling for design of an electrostatic vibration energy harvester's conditioning circuit with an auto-adaptive process to the external vibration changes. In: *Symposium on design, test, integration and packaging of MEMS/MOEMS, 2008. MEMS/MOEMS 2008*, Nice, 9–11 April, pp. 302–306. New York: IEEE.

Guillemet R, Basset P, Galayko D, et al. (2013) Wideband MEMS electrostatic vibration energy harvesters based on gap-closing interdigited combs with a trapezoidal section. In: *2013 IEEE 26th international conference on micro electro mechanical systems (MEMS)*, Taipei, Taiwan, 20–24 January.

Koyama D and Nakamura K (2010) Array configurations for higher power generation in piezoelectric energy harvesting. In: *2009 IEEE international ultrasonics symposium (IUS)*, Rome, 20–23 September, pp. 1973–1976. New York: IEEE.

Mitcheson PD, Yeatman EM, Rao GK, et al. (2008) Energy harvesting from human and machine motion for wireless electronic devices. *Proceedings of the IEEE* 96: 1457–1486.

Nayfeh AH, Lacarbonara W and Chin C (1999) Nonlinear normal modes of buckled beams: three-to-one and one-to-one internal resonances. *Nonlinear Dynamics* 18: 253–273.

Palm WJ (2007) *Mechanical Vibration*. ISBN 978-0-471-34555-8. John Wiley & Sons. UK.

Reddy JN (2004) *Mechanics of Laminated Composite Plates and Shells*. CRC Press, Boca Raton, Florida.

Sebald G, Kuwano H, Guyomar D, et al. (2011) Experimental Duffing oscillator for broadband piezoelectric energy harvesting. *Smart Materials & Structures* 20: 102001.

Shan XB, Yuan JB, Xie T, et al. (2010) Design and experiment of multiple piezoelectric bimorphs for scavenging vibration energy. *International Journal of Applied Electromagnetics and Mechanics* 34: 265–275.

Soliman M, Abdel-Rahman E, El-Saadany E, et al. (2008) A wideband vibration-based energy harvester. *Journal of Micromechanics and Microengineering* 18: 115021.

Stanton SC, McGehee CC and Mann BP (2010) Nonlinear dynamics for broadband energy harvesting: investigation of a bistable piezoelectric inertial generator. *Physica D: Nonlinear Phenomena* 239: 640–653.

Tang L, Yang Y and Soh CK (2010) Toward broadband vibration-based energy harvesting. *Journal of Intelligent Material Systems and Structures* 21: 1867–1897.

Xue H, Hu Y and Wang Q (2008) Broadband piezoelectric energy harvesting devices using multiple bimorphs with different operating frequencies. *IEEE Transactions on Ultrasonics, Ferroelectrics and Frequency Control* 55: 2104–2108.

Yang B, Lee C, Xiang W, et al. (2009) Electromagnetic energy harvesting from vibrations of multiple frequencies. *Journal of Micromechanics and Microengineering* 19: 035001.

Appendix 1

In order to obtain two coupled nondimensional motion equations from equations (6) and (7), the following dimensionless variables are introduced

$$\begin{aligned} \tau &= \omega_0 t \quad q(t) = \sqrt{\frac{|k_1|}{k_3}}\tilde{q}(\tau) \\ \ddot{y}(t) &= \ddot{z}(t) + g \quad y(t) = \sqrt{\frac{|k_1|}{k_3}}\tilde{y}(\tau) \\ V(t) &= \frac{k_1}{\alpha}\sqrt{\frac{|k_1|}{k_3}}\tilde{V}(\tau) \end{aligned} \tag{20}$$

Then, we introduce the following set of parameters

$$\begin{aligned} \omega_0^2 &= \frac{k_1}{M_{eq}} \quad \frac{\vartheta}{M_{eq}} = 2\delta = \frac{\omega_0}{Q} \\ \gamma &= \frac{\omega_0}{\omega_R + \omega_L} \\ k_{em}^2 &= \frac{R_L^2\alpha^2}{k_1 L} = \frac{\lambda^2}{k_1 L} \end{aligned} \tag{21}$$

where $\tilde{k}_{em}^2$ represents the electromechanical coupling factor and γ is the ratio between the linear part of the mechanical resonant frequency and the total cutoff frequency of the electrical circuit.

The corresponding time derivatives of the above variables are given by

$$\begin{aligned} \frac{dq(t)}{dt} &= \omega_0\sqrt{\frac{|k_1|}{k_3}}\frac{d\tilde{q}(\tau)}{d\tau} \quad \frac{d^2q(t)}{dt^2} = \omega_0^2\sqrt{\frac{|k_1|}{k_3}}\frac{d^2\tilde{q}(\tau)}{d\tau^2} \\ \frac{d^2y(t)}{dt^2} &= \omega_0^2\sqrt{\frac{|k_1|}{k_3}}\frac{d^2\tilde{y}(\tau)}{d\tau^2} \\ \frac{dV(t)}{dt} &= \omega_0\frac{k_1}{\alpha}\sqrt{\frac{|k_1|}{k_3}}\frac{dV(\tau)}{d\tau} \end{aligned} \tag{22}$$

By substituting the above new variables and parameters into the governing equations (6) and (7), we obtain

$$\frac{d^2\tilde{q}(\tau)}{d\tau^2} + \frac{1}{Q}\frac{d\tilde{q}(\tau)}{d\tau} + \tilde{q}(\tau) + \tilde{q}^3(\tau) + \tilde{V}(\tau) = -\frac{d^2\tilde{y}(\tau)}{d\tau^2} \tag{23}$$

$$\frac{d\tilde{V}(\tau)}{d\tau} + \frac{1}{\gamma}\tilde{V}(\tau) = k_{em}^2\frac{d\tilde{q}}{d\tau} \tag{24}$$

which are the coupled dimensionless equations of the system with only three independent dimensionless parameters: the mechanical quality factor Q, the cutoff frequency ratio γ and the electromechanical coupling factor k_{em}^2. The time-dependent acceleration signal of the vibration input is represented by the function $d^2\tilde{y}(\tau)/d\tau^2$.